RSC Advances

RSC Publishing

PAPER

View Article Online
View Journal | View Issue

Conformational change-induced switching behavior in pure-carbon systems

Cite this: *RSC Advances*, 2013, **3**, 16672

Yan-Dong Guo,[a] Xiao-Hong Yan*[ab] and Yang Xiao[a]

Received 21st March 2013,
Accepted 9th July 2013

DOI: 10.1039/c3ra41401a

www.rsc.org/advances

Based on first-principles calculation, the electronic transport properties of two–one–two dimensional carbon structures, graphene(benzene)–chain–graphene(benzene), are investigated. Switching behavior induced by conformational changes is observed, even for the systems with curved and quite long carbon chains. The spatial asymmetry of transmission channels between one- and two-dimensional carbon structures is found to be the physical mechanism behind this behavior, and it can be extended to metal systems. It is also found that the orientation of a transmission channel is able to be rotated by a nanotube (or curved graphene) through the non-planar π-conjugated orbitals to modulate the switching behavior. Based on these structures, a kind of extremely-small pure-carbon logic operators and some other devices are proposed. As atomic motion could process information directly, the switching behavior and those devices would be very useful in nanomechanics.

Introduction

Since the measurement of the conductance of a single benzene-1,4-dithiol by Reed *et al.*,[1] molecular devices have attracted more and more attention. Experiments showed that conformational change in molecules would influence their conductance.[2,3] In theory, it is predicted that the twisting of the 4,4′-bipyridine molecule could result in the decay of π–π coupling.[4,5] Based on this feature, some kinds of single-molecule devices have been proposed.[6–21] However, for a long time, electrically controlled twisting in a molecule could not be realized,[22–26] which is essential for the device application. Recently, significant progress has been made in that a single-molecule electric motor has been experimentally demonstrated.[27,28]

Carbon-based nanostructures are the most promising candidates for next-generation electronic devices. Among them, atomic carbon chains and graphene are typical representatives of the one- and two-dimensional (1D and 2D) ones, respectively. Recently, a carbon atomic chain was successfully derived from graphene, forming the 2D–1D–2D structures benzene–chain–benzene (BCB) and graphene–chain–graphene.[29–32] They are a combination of π-conjugated pure-carbon structures with different dimensions, being good candidates for the studies of π coupling. Besides, unlike the former single-molecule device, they are much bigger in structure, with delocalized electrons. In the present work, we focus on the electronic transport properties of these structures. Switching behavior induced by conformational changes (rotating the 2D part) is observed, even for the systems with curved and quite long carbon chains. Further analysis shows that the spatial asymmetry of transmission channels between one- and two-dimensional carbon structures is the underlying physical mechanism, and it can be extended to metal systems. Interestingly, a nanotube or curved graphene could modulate the switching behavior by rotating the spatial orientation of the transmission channel. In particular, we propose a kind of extremely-small pure-carbon logic operators (*e.g.*, NOT, AND, and OR) and some other devices. Different from traditional devices, the atomic motion could process information directly, exhibiting great application potential in nanomechanics.

Methodology

To explore the systems more accurately, density functional theory calculations combined with nonequilibrium Green's function are performed. They are carried out using the Atomistix Toolkit package (ATK).[33,34] We use the mesh cutoff energy of 150 Ry, and 1 × 1 × 100 *k*-point mesh in the Monkhorst–Park scheme.[35] The Perdew–Burke–Ernzerhof (PBE) formulation of the generalized gradient approximation (GGA)[36] to the exchange–correlation functional is used, and the double-zeta polarized basis set is employed in our calculations. Supercell with sufficient vacuum spaces (more than 10 Å) is chosen to prevent the interactions with adjacent images.

For graphene–chain–graphene configuration, we construct the structure of partially hydrogenated graphene layer–chain–partially hydrogenated graphene layer (short for PHGLC,

---

[a] *College of Science, Nanjing University of Aeronautics and Astronautics, Nanjing 210016, China. E-mail: xhyan@nuaa.edu.cn*

[b] *College of Electronic Science and Engineering, Nanjing University of Posts and Telecommunications, Nanjing 210046, China*

shown in Fig. 1), where electrodes are two semi-infinite GNRs.[37,38] It is found that there are two kinds of stable structures considering the contact between graphene and the carbon chain, PHGLC1 and PHGLC2 [Fig. 1(a) and (d)].[29,30] In BCB structures, we use the semi-infinite atomic carbon linear chain as the electrode,[39] which is a good conductor and can eliminate complications that may arise from electrode–molecule interactions.[39] Also, the whole system consists of carbon and hydrogen atoms only and can be seen as a ''pure-carbon'' system. For simplicity, the number n represents the length of the finite carbon chain between the nanoribbons or benzene rings. We optimized the structures until all the forces are less than 0.05 eV Å^{-1}. For the current under a finite bias V_b, it is obtained according to the following function:

$$I(V_b)=\frac{e}{h}\int_{\mu_R}^{\mu_L} T(E,V_b)[f(E-\mu_R)-f(E-\mu_L)]\mathrm{d}E$$

where $T(E,V_b)$ is the transmission spectrum, $f(E - \mu_{L,R})$ is the Fermi function for the left (right) lead, and $\mu_{L,R}$ is the lead's chemical potential. For the bias between two leads, it is $V_b = (\mu_L - \mu_R)/e$, and the Fermi level of the whole system is defined as the average of the chemical potentials of the two leads.

Results and discussion

The switching behavior

In previous molecular switches, an increase in rotation angle θ will result in a decrease in the coupling of the π orbitals, as the benzene rings are adjacent or close to each other. However, in our PHGLC and BCB structures (Fig. 1 and Fig. 2), the carbon chain separates the two aromatic moieties far away from each other. Although the π orbitals are delocalized, the long distance eliminates their direct coupling. As the carbon chain is π-conjugated, it is necessary to investigate the chain-induced effect.

The structures of PHGLC1 and PHGLC2 we studied here are shown in Fig. 1(a) and (d), respectively. Initially, the two GNR planes are parallel to each other. Then, we fix one GNR and rotate another one around the chain [Fig. 1(c)]. As an example, we choose the bias of 1.0 V to see its performance under a finite bias. By increasing the rotation angle θ, the current decreases and finally goes to almost zero [Fig. 1(e)], exhibiting good switching behavior. It should be noted that this behavior is valid for all four cases, indicating it is an intrinsic feature of such systems. Moreover, the currents of odd-numbered chains (PHGLC1 and PHGLC2; n = 9) are higher than that of even-numbered ones (PHGLC1 and PHGLC2; n = 10). This is due to the odd–even effect.[39–41] For these structures, near the end atoms of the chains, the bond lengths are almost the same between the odd and even cases.[42] But for the inner atoms, even chains exhibit larger bond length alternation than odd ones.[42] As a result, the even and odd chains in our systems could be seen as ''polyyne-like'' and ''cumulene-like'' structures, exhibiting low and high conductances respectively.[16,43]

For a BCB device (Fig. 2), we calculated larger n cases, as less computational cost is required due to the decreasing atom numbers. Apparently, the benzene ring plays the same role as

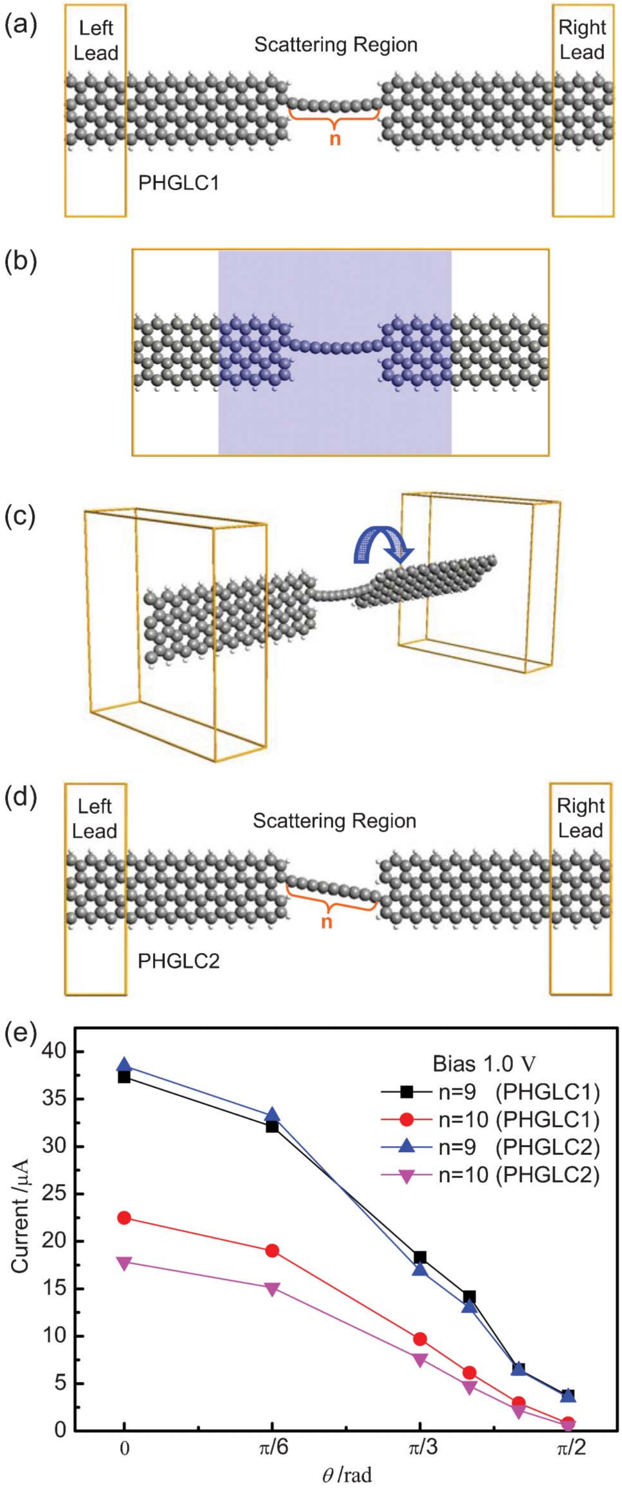

Fig. 1 (a) The configuration of a 2D–1D–2D PHGLC1 device. The left and right supercells indicate the semi-infinite electrodes. The scattering region includes the 2D–1D–2D structure and several layers of electrodes for screening purposes. (b) Take the configuration in (a) as an example to show the optimization, where the scattering region is seen as a periodic geometry. The atoms within the shaded region are fully relaxed and others are frozen. (c) Illustration of rotation. Due to the large vacuum layers (more than 10 Å), the rotation will not destroy the periodic condition or induce extra interaction between adjacent images. (d) The configuration of a PHGLC2 device. (e) Switching performances of PHGLC1 and PHGLC2. The currents are obtained under a bias of 1.0 V.

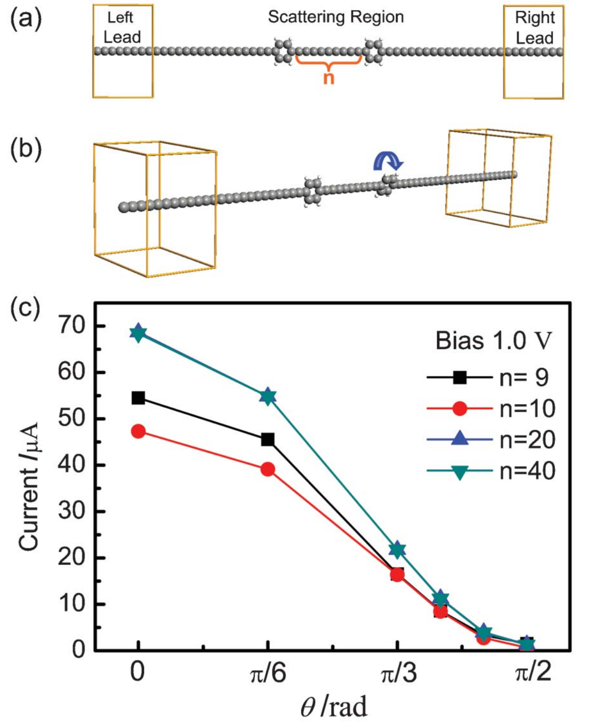

Fig. 2 (a) The configuration of a BCB 2D–1D–2D device. The left and right supercells indicate the left and right semi-infinite electrodes, respectively. (b) The illustration of rotating the right ring (the left one is fixed) for BCB. (c) Switching performance of BCB. The currents are obtained under a bias of 1.0 V with different rotation angles θ.

GNR. Actually, from the structural point of view, a benzene ring can be seen as the narrowest and shortest GNR. They are both 2D structures and both formed by the big π orbital. As the GNR and benzene ring can play the same role in such 2D–1D–2D carbon systems, to save computational cost, we use a benzene ring instead of GNR in the following calculation and discussion. One thing should be noted, that the benzene ring can be replaced by GNR and achieve the same effect. Compared with PHGLC, the current in BCB [Fig. 2(c)] is higher. We attribute this difference to the conductance gap in a symmetric GNR induced by bias.[40] Actually, the most important feature of such 2D–1D–2D systems is the relative conductance changing trend varying with θ. For $n = 20$ and 40 cases in Fig. 2(c), the carbon chains are long enough to be analogous to the infinite chain,[30] which is a better conductor than the single-atom gold chain,[39] so the currents exhibit no attenuation from $n = 20$ to 40 and are even higher than that of the $n = 9$ and 10 cases. If we make high conductance represent ''1'' and low, ''0'', we can use it for data transfer for long distances, which will be very useful in nanoelectronic devices. In addition, we can also use it as a large-distance angle detector. The two benzene rings can be placed far away, and they work as ''angle polarizer'' and ''angle analyzer'', respectively.

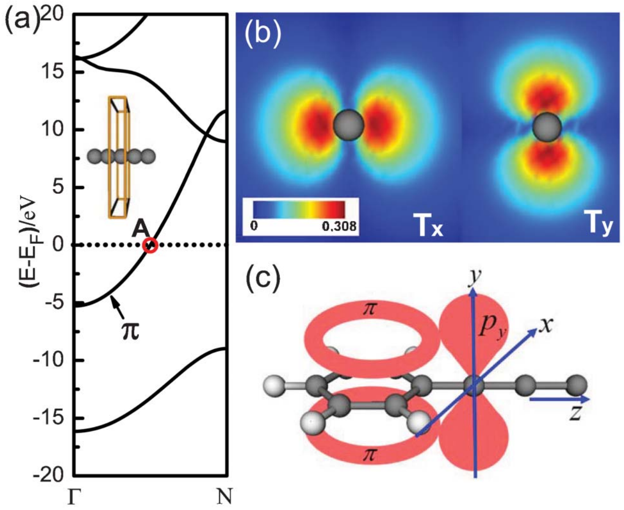

Fig. 3 (a) Energy band of infinite carbon linear chain. (b) Contour plots of transmission eigenchannels T_x and T_y of the carbon chain at the Fermi energy (point A) in the cross-section. (c) Schematic for the orbital coupling between the benzene ring and carbon chain.

The switching mechanism

In order to figure out the physical mechanism behind this, we focus on the basic parts of the system. For an infinite carbon chain, at the Fermi energy, there are two degenerate π bands [Fig. 3(a)], arising from the π_x and π_y orbitals.[39] These two orbitals are formed by the p_x and p_y atomic orbitals, and contribute to two transmission eigenchannels, T_x and T_y [Fig. 3(b)], respectively. Thus, they both exhibit the dumbbell shape of the p orbital, determining how the current flows in the device. As for the eigenchannel, it means there will be no current flowing from one to another, so we could research each one independently. When inserting a ring [Fig. 3(c)], one eigenchannel remains open and the other is blocked, due to the 2D structure and its corresponding large π orbital. As we can see, in Fig. 3(c), the p_y orbital of the carbon chain couples with the π orbital of the ring, but there is nothing for the p_x orbital to couple with.

This block-effect could be clearly seen from the change in the transmission spectrum. For the infinite carbon chain, the transmission spectrum is shown in Fig. 4 (solid line). We can see that, in the energy range of −2.0 to +2.0 eV, the transmission coefficient is exactly 2.0, indicating the two eigenchannels are totally opened (each for 1.0, *i.e.*, 100%). The table of transmission eigenvalues in Fig. 4 confirms this: for a bare carbon chain, the eigenvalue is almost 1.0 for each of the two eigenchannels. When inserting a benzene ring into the chain, the transmission decreases to about 1.0 (dashed line). As shown in the table in Fig. 4, the first eigenchannel remains open and the second one is totally blocked. So the total transmission coefficient is now about 1.0, *i.e.*, only the first eigenchannel contributes to the transmission. Three dimensional distribution of this opened eigenchannel at the Fermi energy is also plotted (the inset in the bottom right of Fig. 3, and the benzene plane is perpendicular to the paper). From that, we can clearly see the first eigenchannel can be

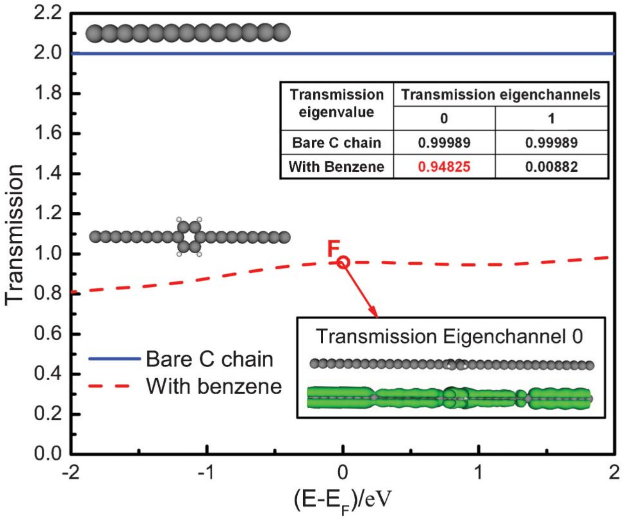

Transmission eigenvalue	Transmission eigenchannels	
	0	1
Bare C chain	0.99989	0.99989
With Benzene	0.94825	0.00882

Fig. 4 Transmission spectra and eigenchannels of a bare infinite carbon chain and the chain with a benzene ring. The solid (blue) and dashed (red) lines represent the transmission spectra for bare carbon chain and the chain with a benzene ring, respectively. Inset table shows the corresponding transmission eigenvalues of the first and second transmission eigenchannels for the two cases at the Fermi energy. The inset on bottom right shows the three dimensional distribution of the first eigenchannel for the chain with a benzene ring at the Fermi energy (the ring's plane is perpendicular to the paper).

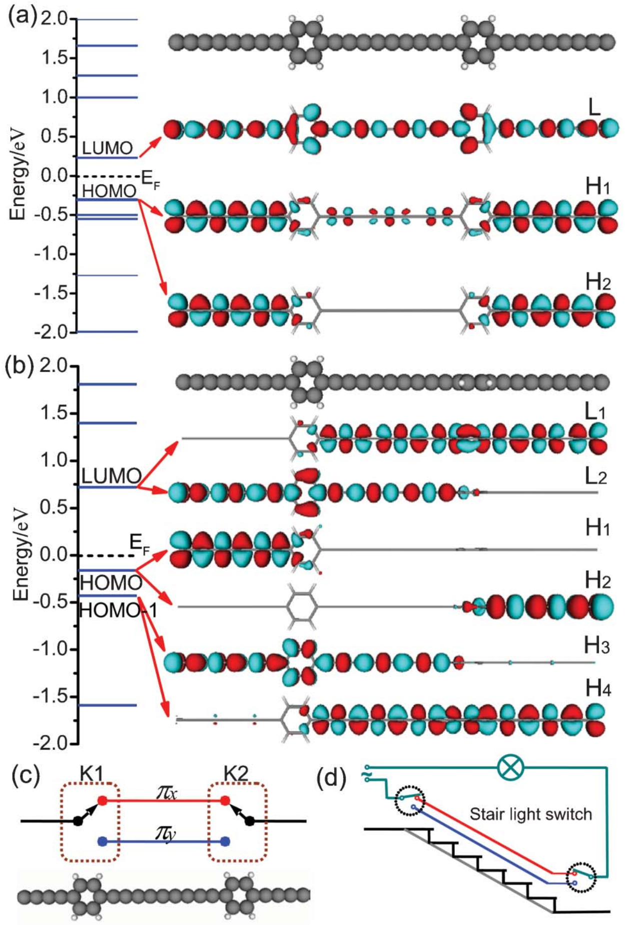

Fig. 5 (a) Energy spectrum and spatial distributions of LUMO and HOMO states for the parallel case of BCB (HOMO states are doubly degenerate). (b) Energy spectrum and spatial distributions of LUMO, HOMO, and HOMO-1 states for the perpendicular case of BCB (all are doubly degenerate). (c) Schematic of the two channels switch. (d) Schematic of stair light switch.

distributed throughout the whole system, which is contributed by one of the p orbital components which has a consistent spatial orientation with the π orbital of the ring.

We next insert two rings to form the BCB structure. Striping off electrodes (semi-infinite carbon chains), we focus on the middle scattering region, and plot its energy spectrum and the spatial distributions of orbitals near the Fermi energy in Fig. 5. It is these orbitals that contribute to the transmission. For the parallel case [Fig. 5(a)], there are one lowest unoccupied molecular orbital (LUMO) and two degenerate highest occupied molecular orbitals (HOMOs). As one finds, the two HOMO orbitals are blocked because the spatial orientation is not consistent with the large π orbitals of the rings. Only the LUMO orbital (L) is distributed throughout the molecule and dominates the transmission. For the perpendicular case [Fig. 5(b)], there are doubly degenerate LUMO, HOMO, and HOMO-1 orbitals, but all of them are blocked. According to the orientation, all the orbitals can be divided into two categories. Whether an orbital can be distributed throughout the whole system or not depends on the orientations of the orbital itself and the two rings. When the orbital encounters a ring which has the same orbital orientation, it can go through; otherwise, it stops there. For instance the orbital H_3 in Fig. 5(b), from left to right: it can go through the first ring but stops at the second one. Such behavior could be found for all the orbitals in Fig. 5.

Actually, we can interpret this behavior in a simple way. If we regard each transmission eigenchannel as a conducting wire [π_x and π_y, Fig. 5(c)], then each ring behaves like a single-pole double throw switch. Rotating by π/2 is equivalent to switching to another pole. The 2D–1D–2D system is similar to the stairway light switch in Fig. 5(d). Only when the two switches are thrown to the same wire, could the system be conductible.

When we rotate one of the aromatic moieties from the $\theta = 0$ or $\pi/2$ case, it is easy to see that not only a decoupling from the corresponding parallel π orbital (with respect to that aromatic moiety), but also a coupling with the perpendicular π orbital would take place. As a result, for the cases of $0 < \theta < \pi/2$, each aromatic moiety would have couplings with both of the two π orbitals.

Next, we show how the orbitals change with torsion angle and chain length. Here, Fig. 6 shows the HOMO and LUMO orbitals of BCB varying with torsion angle (left panel) and chain length (right panel). Interestingly, as the torsion angle increases, the LUMO orbital is twisted (left panel in Fig. 6). That is to say, the partial coupling of π orbitals (or in other words, the orbital projection) is not localized at the 2D–1D interfaces, but is distributed evenly all over the chain. When the chain length increases, the HOMO orbitals may take part in the electronic transmission ($n = 7$ and 10), *i.e.*, the orbital is distributed throughout the device. However, surprisingly, no

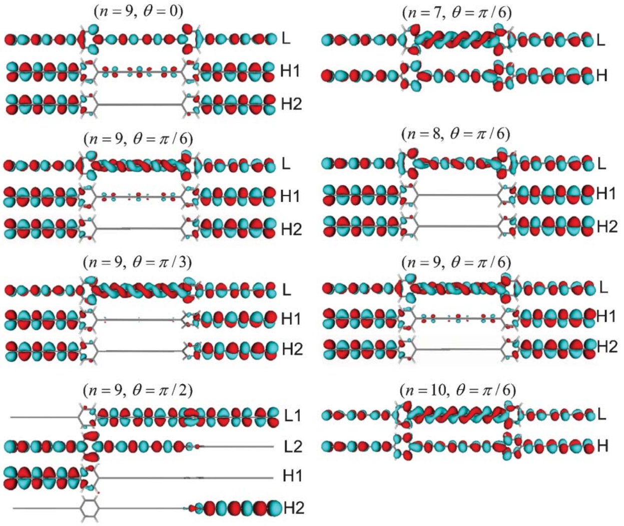

Fig. 6 The left panel shows the HOMO (HX, and X for degenerate orbitals) and LUMO (LX) orbitals for BCB structures with $n = 9$ and different θ. The right panel shows the HOMO (HX) and LUMO (LX) orbitals for BCB structures with $\theta = \pi/6$ and different lengths.

orbital twisting phenomenon is observed in the HOMO orbitals.

According to previous studies, the carbon linear chain is stiff along the axis but flexible in transverse directions.[21] It can form curved and helical structures.[21] One expects that the switching behavior can still exist in these flexible structures, where the devices can adapt to complex environments and be very useful for circuit design. Furthermore, they can extend the devices to three dimensional ones, which is a promising research direction for nanoelectronic devices. For our system, Fig. 7 shows the performance after being inserted with curved and helical carbon chains. For small rotation angles, the current with a curved chain is a little higher than that of the helical one, but the switching behavior remains unchanged for both cases, where the currents still decrease with the increasing of θ. Compared with straight ones, the flexible carbon chain structures do not degrade the switching performance of the device.

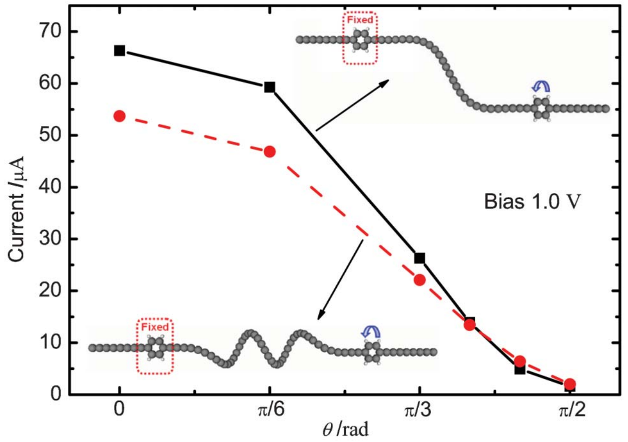

Fig. 7 The performances of BCB with curved chain (black solid line with squares) and helical chain (red dashed line with circles) under a bias of 1.0 V. The corresponding rotation angles are 0, π/6, π/3, 7π/18, 4π/9 and π/2, respectively.

Extremely-small pure-carbon logic operators

Based on the studies above, we propose a more useful application, *i.e.*, logic gates. With 2D–1D–2D structures, we design three basic logic gates, NOT, AND, and OR. Fig. 8(a) shows the NOT gate and the corresponding truth table. For it, the inputs are the orientations of the benzene plane: parallel

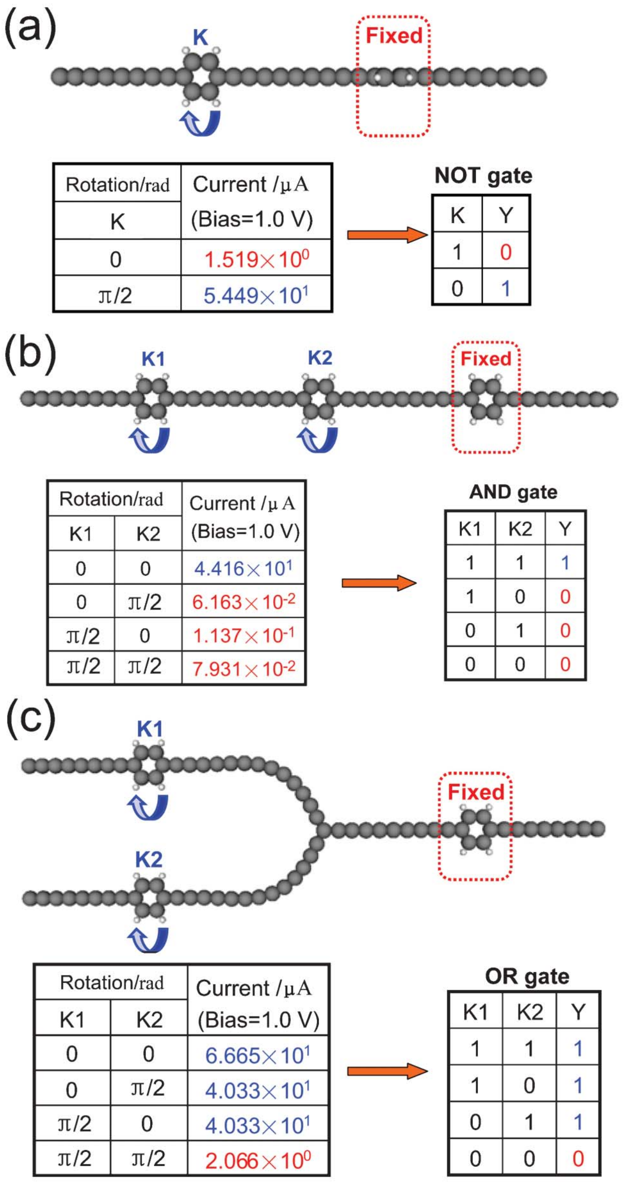

NOT gate

Rotation/rad K	Current /μA (Bias=1.0 V)
0	1.519×10^{0}
π/2	5.449×10^{1}

K	Y
1	0
0	1

AND gate

Rotation/rad K1	K2	Current /μA (Bias=1.0 V)
0	0	4.416×10^{1}
0	π/2	6.163×10^{-2}
π/2	0	1.137×10^{-1}
π/2	π/2	7.931×10^{-2}

K1	K2	Y
1	1	1
1	0	0
0	1	0
0	0	0

OR gate

Rotation/rad K1	K2	Current /μA (Bias=1.0 V)
0	0	6.665×10^{1}
0	π/2	4.033×10^{1}
π/2	0	4.033×10^{1}
π/2	π/2	2.066×10^{0}

K1	K2	Y
1	1	1
1	0	1
0	1	1
0	0	0

Fig. 8 (a)–(c) The structures, performances and truth tables for logic gates NOT, AND, and OR, respectively. Inputs are the orientations of the benzene plane: being parallel to the paper ($\theta = 0$) represents ''1'', and perpendicular ($\theta = \pi/2$) represents ''0''. For output: being conductible (high conduction with large current) represents ''1'', and non-conductible (blocked with very small leakage current) represents ''0''.

to the paper (rotation angle $\theta = 0$) represents "1", and perpendicular (rotation angle $\theta = \pi/2$) represents "0". For output: conductible (high conduction with large current) represents "1", and non-conductible (blocked with very small leakage current) represents "0". For NOT gate, we fix the right ring and make its plane perpendicular to the paper. Under the bias of 1.0 V, the current for input "1" is almost zero, while a finite value for input "0". According to the rules, we get output "1" for input "0", and get output "0" for input "1", *i.e.*, NOT gate.

When we insert three rings into the chain, and place them initially as shown in Fig. 8(b), then we get the AND gate. Apparently, only when all the rings are parallel, the system can be conductible. That is to say, only when both of the inputs are "1", will the output be "1", *i.e.*, AND gate. The calculated result in Fig. 8(b) demonstrates our analysis. Perhaps the most interesting challenge is the design of an OR gate. The output is "1" if at least one of the inputs is "1". Now, one chain is not enough. Since the carbon chain can branch off to form a T junction,[39] we construct the OR gate with the setup shown in Fig. 8(c). When at least one of the left two rings is parallel to the fixed ring, there will be current, *i.e.*, output "1". The simulated result in Fig. 8(c) confirms this. As we know, any other gate can be achieved by combining the above three basic gates. Actually, some gates can also be designed directly. For instance, if we change the fixed ring in Fig. 8(b) to be perpendicular to the paper, then we get a NOR gate.

Compared with previous logic gates, there are four clear advantages for our gates. First, they are pure-carbon ones, which is a promising direction for future nanoelectronic devices. Second, the width is very small (only one atom thick for the narrowest part). Third, as the device is robust to the shape and length of the chain, it is useful for circuit design and can be extended to three dimensions. Fourth, they are very useful in nanomechanics, as the atomic motion can process information directly.

For molecular logic gates, one of the challenges is to establish the logic gate system, where the output of one gate can be used as the input of another.[44] Actually, this is the foundation of molecular computing. In the above studies, we use atomic motion to control electricity. Now, the problem becomes how to use electricity to control atomic motion. In theory, by doping, the 2D carbon structure can be polarized and rotated by an electric field.[16,17,37,39,45] But this electrically-controlled atomic twisting could not be realized for a long time. Recently, significant progress has been made. Leoni *et al.*[27] realized a new electromechanical single-molecular switch through rotating the molecule by applying a small voltage, and Tierney *et al.*[28] demonstrated a single-molecule electric motor also by a small voltage. For our gates, when applying bias, the output lead will be at high or low electric potential. So, we can use it to rotate the ring of another gate. Thus, the output can be used as another gate's input, establishing the logic gate system.

To figure out the doping effect on the devices, Fig. 9 shows the performance of the device(s) doped with nitro (and amino) group(s). As we can see, after doping, the rotation induced switching behavior still exists, because the 2D structural properties of the ring do not change. Thus, as long as the 2D structure of the ring is not destroyed, some other functional groups can also be doped in the ring and will retain the switching behavior.

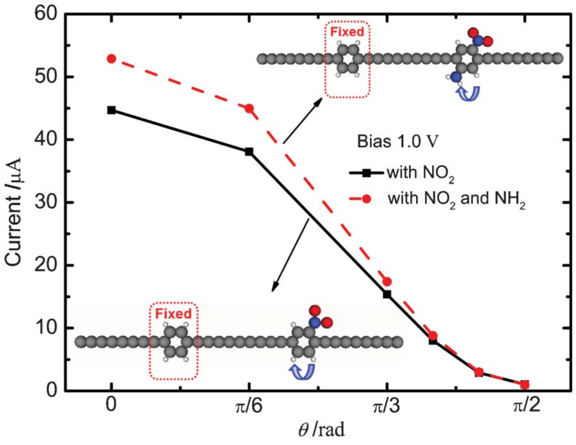

Fig. 9 Switching performances of the BCB devices doped with functional groups. Black (solid) line with squares represents the case doped with nitro group, and red (dashed) line with circles represents the case doped with both nitro and amino groups.

The cos$^2(\theta)$ relation and its modulation

For the BCB devices with $0 < \theta < \pi/2$, the coupling between the orbitals or transmission channels of the chain and rings plays an import role. Previous studies showed that, when the rotation angle of the π-conjugated molecule increases, the π–π coupling strength will decay following a cos(θ) law.[4,5] For the junction conductance, it will decrease following a cos$^2(\theta)$ law,[18,46] as the electron transfer rates scales as the square of the π-overlap, and this has been proved by experiment.[7,47–49] For our BCB system, the fitting function and corresponding curve are shown in Fig. 10. Apparently, the curve follows the cos$^2(\theta)$ relation quite well. As a result, the middle chain can be neglected, and the orbitals of the two rings act as coupling to

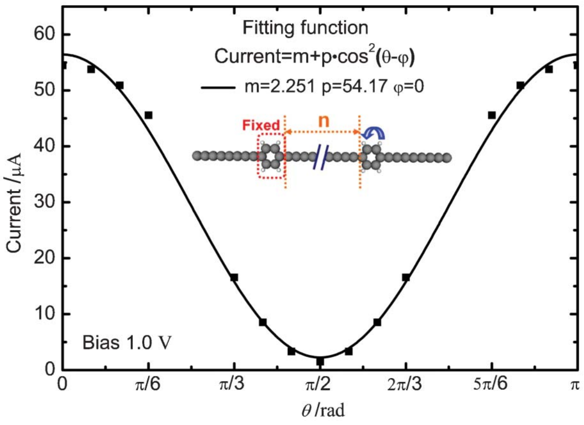

Fig. 10 Fitting function for the current–angle relation in BCB device with $n = 9$. The fitting function and parameters are shown in the figure, and the curve follows the cos$^2(\theta)$ relation.

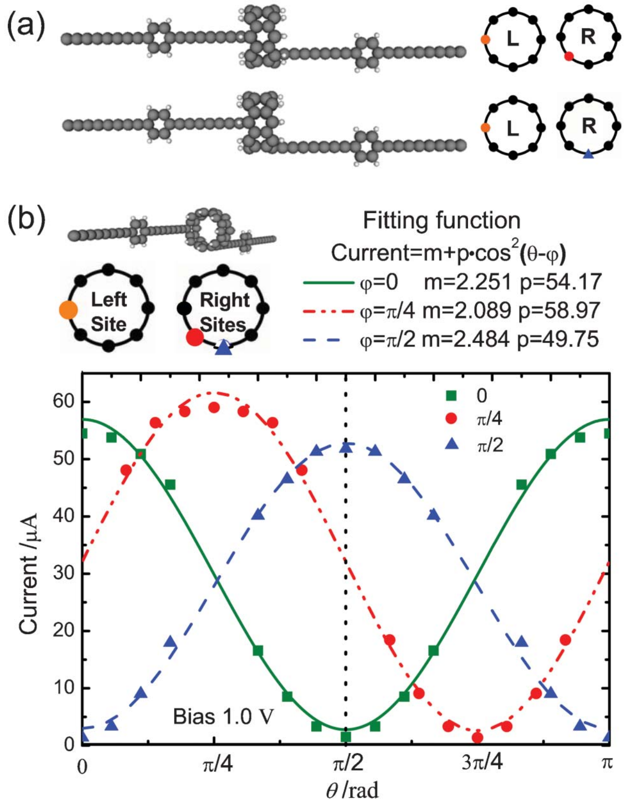

Fig. 11 Tunnel-orientation rotators. (a) The structures of rotators for rotating tunnel orientation in $\varphi = \pi/4$ and $\pi/2$. The left contact site is denoted by the ring, and the right contact sites are denoted by the circle and triangle for $\pi/4$ and $\pi/2$, respectively. (b) Corresponding currents, fitting function, and fitting curves. $\varphi = 0$ corresponds to the non-nanotube case (see Fig. 10).

each other directly. This is because the whole carbon chain is π-conjugated throughout.

Depending on the nanoelectronic devices, treating the exchange–correlation potential at a higher level of approximation might have an effect. Here, we prove that, for our system, the results at PBE level are reliable. In all kinds of our devices, the fundamental mechanism is the $\cos^2(\theta)$ relation. The good agreement suggests that the PBE level could give a good description of our system and reveal its key mechanism. There is no need to use a higher level of approximation, and the effect, which might be induced by it, is not dominant. In addition, we also checked our results using the self-interaction corrected LDA (LDA.PZ),[50] and good agreement with the $\cos^2(\theta)$ relation is obtained (not shown).

From the structural point of view, a nanotube can be seen as curved by the 2D structure of GNR. As a result, the distribution of the π orbital will also follow the wall of the tube during the curving process. Here, we insert a finite (8, 0) nanotube into the BCB structure (Fig. 11). The left chain is fixed to contact with a site on the tube. We move the right chain to contact with different sites on the tube. Then, on the nanotube, the tangent planes of left and right contact sites form an angle φ. Fig. 11(a) shows the structures of $\varphi = \pi/4$ and $\pi/2$ cases. As the orientation of the π orbital changes for different contact sites, the switching behavior should also change. The performance of the device is shown in Fig. 11(b), including the currents ($V_b = 1.0$ V) and corresponding fitting curves. For comparison, the non-nanotube case is also plotted ($\varphi = 0$, the same as that of Fig. 10). Obviously, the $\cos^2(\theta)$ relation still exists after inserting the nanotube. In particular, the I–θ curves are translated exactly by φ along the angle axis (compared to the non-nanotube case, *i.e.*, $\varphi = 0$ case), respectively. As a matter of fact, the orientation of the transmission tunnel can be rotated in an angle φ by a nanotube, without destroying the $\cos^2(\theta)$ relation. It can be used as a tunnel-orientation rotator. This is just an example, it is natural to think that, if we choose a curved GNR or some other chiral nanotubes, any φ can be achieved. This will be very useful in the design of future nanodevices.

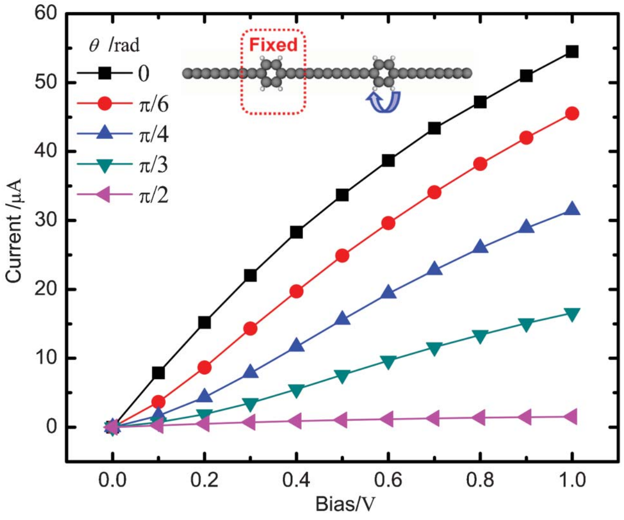

Fig. 12 I–V curves of current amplifier. The corresponding rotation angles are 0, $\pi/6$, $\pi/4$, $\pi/3$, and $\pi/2$, respectively.

In another way, we can take advantage of the rotation angle–conductance relation to design an amplifier. For the BCB device, we apply a series of bias voltages with different rotation angles, and show the corresponding I–V curves in Fig. 12. In each curve, the current increases smoothly with the increase in bias. For each bias, the current also increases smoothly with the decrease in rotation angle. It works well as a current amplifier. Previous studies also reported a similar amplifier, which are realized in a molecule.[6,39] The two benzene rings are adjacent or near, where the orbitals of the two rings can overlap with each other, and the performance is explained by the change in their coupling, while, in our BCB structure, the two benzene rings are far away, and there is no direct interaction between them. For a 1D carbon chain, there are two orthogonal transmission channels, and for a 2D ring, only one transmission channel. It is the spatial asymmetry of the transmission channels between 1D and 2D structures that makes our system work. This is the main difference from previous studies. In addition, the carbon chain between two benzene rings is not only a lead, but also a part of the device. This can be used as a kind of ''delocalized'' device, different from former devices which are localized in an area with outside leads to transfer signals.

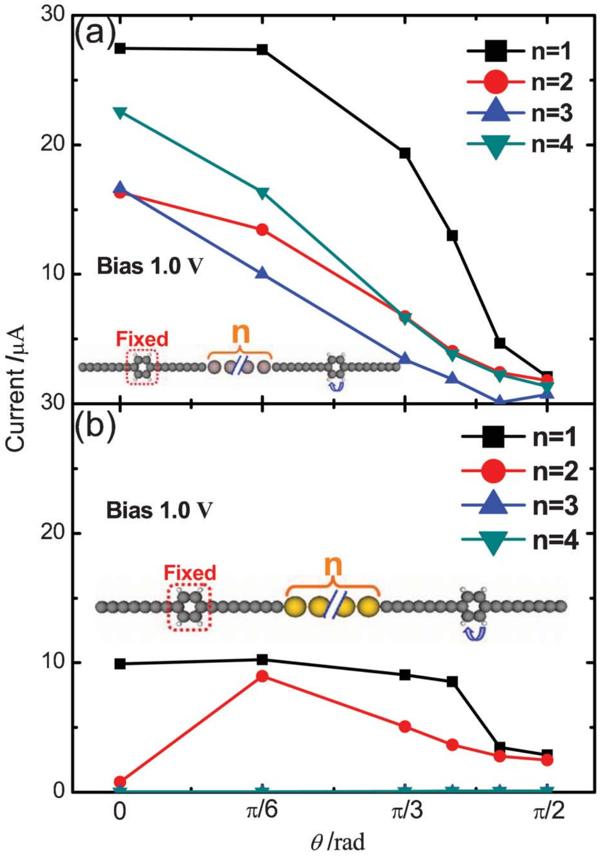

Fig. 13 The performances of BCB with inserted metal atoms under bias of 1.0 V for (a) Al and (b) Au. The number of inserted metal atoms is one to four. The corresponding rotation angles are 0, π/6, π/3, 7π/18, 4π/9 and π/2, respectively.

Extension to metal systems

In GCG or BCB structures, the two orthogonal transmission eigenchannels originate from the p_x and p_y orbitals of the carbon atoms. In principle, other elements which have similar valence electron orbitals should also work in such a 2D–1D–2D structure. Au, Ag, Cu, and Al are the most commonly used metal electrode materials. Among them, Al has a p electron to be the valence electron, but for Au, Ag, and Cu, it is the s electron. Here, Al and Au are chosen as representatives for each category and they are inserted into the carbon chain of BCB (see the insets of Fig. 13). For the Al-doped case, the performance of the device is shown in Fig. 13(a). We find that the switching behavior still exists, for all the four cases with different numbers of Al atoms. No doubt, the p orbital of Al plays the same role as that of C. So, the p orbital induced switching effect is not only a property existing in carbon systems, but also a general one in other p orbital systems. Thus, some other interesting devices can be designed.

For the case of Au, the valence electron is an s electron. Fig. 13(b) shows the performance of the system when we insert one to four Au atoms. This time, the result is quite different. For the cases with one and two Au atoms, there is no clear trend for the relationship between current and θ. For $n = 3$ and 4 cases, there is no current at all, where the transmission channels are totally blocked. The switching feature disappears. We argue that, due to the highly delocalized nature of the π-electron cloud, the orbitals of the carbon atoms can get across one or two Au atoms to overlap with each other, but the distance of three or four Au atoms is too great to cross for the π orbital. Moreover, there is an energy mismatch between C and Au chains, and a barrier will form at the interface.[7,13] Thus, the current decreases (even to almost zero) as the number of Au atoms increases. In brief, the rotation induced switching effect can not work in s orbital systems, as it is isotropic in the x–y plane.

Discussion of device operation and practical application

Finally, we want to discuss the operation and application of the devices. Due to the channel blockage and structural properties, scattering would mainly occur at the 2D–1D junctions, while, according to the switching (Fig. 1 and Fig. 2) performance and gate (Fig. 8) performances, the scattering only affects the device very slightly. For the electrode material, we use carbon structures (semi-infinite GNR or carbon chains) in this paper. Since the device needs to be in contact with metal in some practical cases, *e.g.*, the metal electrodes, these effects should be considered. For this, we have demonstrated above that metal with a p orbital can work well by direct contact. Besides, previous studies showed that the anchoring atom, *e.g.*, sulfur, can link the metal electrode and carbon-switching device well.[20] Furthermore, in order to ensure the application, our calculations are carried at 300 K, since the scattering induced by high temperature would cause intercoupling between the T_x and T_y transmission channels.

Conclusions

In summary, we have investigated the switching behavior induced by conformational changes in 2D–1D–2D pure-carbon structures. The spatial asymmetry of transmission channels between one- and two-dimensional carbon structures is found to be the underlying physical mechanism, and it can be extended to metal systems. A kind of extremely-small pure-carbon logic gates, *i.e.*, NOT, AND, and OR, is proposed by these structures, and a corresponding logic gate system could be established for computing. Moreover, some other useful devices are also proposed in this mechanism, *e.g.*, data transfer and tunnel-orientation rotator. The switching feature and these devices would be very useful in nanomechanics, as the atomic motion can process information directly.

Acknowledgements

This work is supported by the National Natural Science Foundation of China (NSFC10874089, NSFC51032002, and NSFC11247033), the key project of National High Technology Research and Development Program of China (2011AA050526), the Funding of Jiangsu Innovation Program for Graduate Education (CXZZ11_0190 and CX08B_005Z), and the

Fundamental Research Funds for the Central Universities (NS2012005 and NS2012064).

References

1 M. Reed, C. Zhou, C. Muller, T. Burgin and J. Tour, *Science*, 1997, **278**, 252.
2 Z. Donhauser, B. Mantooth, K. Kelly, L. Bumm, J. Monnell, J. Stapleton, D. Price Jr, A. Rawlett, D. Allara and J. Tour, *Science*, 2001, **292**, 2303.
3 F. Moresco, G. Meyer, K.-H. Rieder, H. Tang, A. Gourdon and C. Joachim, *Phys. Rev. Lett.*, 2001, **86**, 672.
4 S. Woitellier, J. Launay and C. Joachim, *Chem. Phys.*, 1989, **131**, 481–488.
5 S. Larsson, *J. Am. Chem. Soc.*, 1981, **103**, 4034–4040.
6 M. Reed and J. Tour, *Sci. Am.*, 2000, **283**, 86.
7 L. Venkataraman, J. Klare, C. Nuckolls, M. Hybertsen and M. Steiger-wald, *Nature*, 2006, **442**, 904–907.
8 J. M. Seminario, P. A. Derosa and J. L. Bastos, *J. Am. Chem. Soc.*, 2002, **124**, 10266–10267.
9 L. Senapati, R. Pati and S. C. Erwin, *Phys. Rev. B: Condens. Matter Mater. Phys.*, 2007, **76**, 024438.
10 S. Quek, M. Kamenetska, M. Steigerwald, H. Choi, S. Louie, M. Hybert-sen, J. Neaton and L. Venkataraman, *Nat. Nanotechnol.*, 2009, **4**, 230–234.
11 M. Magoga and C. Joachim, *Phys. Rev. B: Condens. Matter*, 1999, **59**, 16011.
12 M. P. Samanta, W. Tian, S. Datta, J. I. Henderson and C. P. Kubiak, *Phys. Rev. B: Condens. Matter*, 1996, **53**, R7626.
13 L. Wang, Y. Guo, C. Tian, X. Song and B. Ding, *Phys. Lett. A*, 2010, **374**, 4876–4879.
14 C. Xia, C. Fang, P. Zhao and D. Liu, *Curr. Appl. Phys.*, 2010, **10**, 848–852.
15 J. Lu, J. Wu, H. Chen, W. Duan, B. Gu and Y. Kawazoe, *Phys. Lett. A*, 2004, **323**, 154–158.
16 F. Jiang, Y. Zhou, H. Chen, H. Mizuseki and Y. Kawazoe, *Phys. Lett. A*, 2006, **359**, 487–493.
17 R. Pati and S. P. Karna, *Phys. Rev. B: Condens. Matter Mater. Phys.*, 2004, **69**, 155419.
18 Y. Li, J. Zhao and G. Yin, *Comput. Mater. Sci.*, 2007, **39**, 775–781.
19 X. Chen, Y. Xu and Z. Zeng, *Phys. B*, 2008, **403**, 2597–2601.
20 I. Cacelli, A. Ferretti, M. Girlanda and M. Macucci, *Chem. Phys.*, 2006, **320**, 84–94.
21 I. Cacelli, A. Ferretti, M. Girlanda and M. Macucci, *Chem. Phys.*, 2007, **333**, 26–36.
22 J. Seldenthuis, F. Prins, J. Thijssen and H. van der Zant, *et al.*, *ACS Nano*, 2010, **4**, 6681.
23 P. Kŕal and T. Seideman, *J. Chem. Phys.*, 2005, **123**, 184702.
24 H. Kitagawa, Y. Kobori, M. Yamanaka, K. Yoza and K. Kobayashi, *Proc. Natl. Acad. Sci. U. S. A.*, 2009, **106**, 10444–10448.
25 R. D. Astumian, *Proc. Natl. Acad. Sci. U. S. A.*, 2005, **102**, 1843–1847.
26 D. Dundas, E. J. McEniry and T. N. Todorov, *Nat. Nanotechnol.*, 2009, **4**, 99–102.
27 T. Leoni, O. Guillermet, H. Walch, V. Langlais, A. Scheuermann, J. Bon-voisin and S. Gauthier, *Phys. Rev. Lett.*, 2011, **106**, 216103.
28 H. L. Tierney, C. J. Murphy, A. D. Jewell, A. E. Baber, E. V. Iski, H. Y. Khodaverdian, A. F. McGuire, N. Klebanov and E. C. H. Sykes, *Nat. Nanotechnol.*, 2011, **6**, 625–629.
29 A. Chuvilin, J. Meyer, G. Algara-Siller and U. Kaiser, *New J. Phys.*, 2009, **11**, 083019.
30 C. Jin, H. Lan, L. Peng, K. Suenaga and S. Iijima, *Phys. Rev. Lett.*, 2009, **102**, 205501.
31 J. Meyer, C. Girit, M. Crommie and A. Zettl, *Nature*, 2008, **454**, 319–322.
32 L. Ravagnan, N. Manini, E. Cinquanta, G. Onida, D. Sangalli, C. Motta, M. Devetta, A. Bordoni, P. Piseri and P. Milani, *Phys. Rev. Lett.*, 2009, **102**, 245502.
33 J. Taylor, H. Guo and J. Wang, *Phys. Rev. B: Condens. Matter Mater. Phys.*, 2001, **63**, 245407.
34 M. Brandbyge, J. L. Mozos, P. Ordejon, J. Taylor and K. Stokbro, *Phys. Rev. B: Condens. Matter Mater. Phys.*, 2002, **65**, 165401.
35 H. J. Monkhorst and J. D. Pack, *Phys. Rev. B: Solid State*, 1976, **13**, 5188.
36 J. P. Perdew, K. Burke and M. Ernzerhof, *Phys. Rev. Lett.*, 1996, **77**, 3865.
37 L. Shen, M. Zeng, S. Yang, C. Zhang, X. Wang and Y. Feng, *J. Am. Chem. Soc.*, 2010, **132**, 11481–11486.
38 M. Zeng, L. Shen, Y. Cai, Z. Sha and Y. Feng, *Appl. Phys. Lett.*, 2010, **96**, 042104.
39 S. Tongay, R. T. Senger, S. Dag and S. Ciraci, *Phys. Rev. Lett.*, 2004, **93**, 136404.
40 N. D. Lang and P. Avouris, *Phys. Rev. Lett.*, 2000, **84**, 358.
41 N. D. Lang and P. Avouris, *Phys. Rev. Lett.*, 1998, **81**, 3515.
42 Z. Zanolli, G. Onida and J. C. Charlier, *ACS Nano*, 2010, **4**, 5174–5180.
43 J. A. Frst, M. Brandbyge and A. P. Jauho, *Europhys. Lett.*, 2010, **91**, 37002.
44 T. Carell, *Nature*, 2011, **469**, 45–46.
45 A. Nitzan, *Annu. Rev. Phys. Chem.*, 2001, **52**, 681–750.
46 Z. Li, H. Qian, J. Wu, B.-L. Gu and W. Duan, *Phys. Rev. Lett.*, 2008, **100**, 206802.
47 G. H. Ma, X. Shen, L. L. Sun, R. X. Zhang, P. Wei, S. Sanvito and S. M. Hou, *Nanotechnology*, 2010, **21**, 495202.
48 S. Woitellier, J. Launay and C. Joachim, *Chem. Phys.*, 1989, **131**, 481–488.
49 V. Mujica, A. Nitzan, Y. Mao, W. Davis, M. Kemp, A. Roitberg and M. A. Ratner, in *Electron Transfer in Molecules and Molecular Wires: Geometry Dependence, Coherent Transfer, and Control*, John Wiley & Sons, Inc., 2007, pp. 403–429.
50 J. P. Perdew and A. Zunger, *Phys. Rev. B*, 1981, **23**, 5048–5079.